Chemical Engineering Journal 501 (2024) 157776

Contents lists available at ScienceDirect

Chemical Engineering Journal

journal homepage: www.elsevier.com/locate/cej

Nonthermal hydrogen plasma-enabled ambient, fast lignin hydrogenolysis to valuable chemicals and bio-oils

Parsa Pishva [a], Jialu Li [b], Rongxuan Xie [a], Jinyao Tang [a], Prangan Nandy [c], Tanvir Farouk [c], Jinghua Guo [b], Zhenmeng Peng [a,*]

[a] Department of Chemical Engineering, University of South Carolina, Columbia, SC 29208, United States
[b] Advanced Light Source, Lawrence Berkeley National Laboratory, Berkeley, CA 94720, United States
[c] Department of Mechanical Engineering, University of South Carolina, Columbia, SC 29208, United States

ARTICLE INFO

Keywords:
Lignin
Fast hydrogenolysis
Nonthermal plasma
Biomass conversion

ABSTRACT

The reduction of fossil fuel resources and the ongoing surge in global energy demand have captured the interest of researchers worldwide, prompting a focus on developing renewable energy sources. For this reason, biomass conversion has emerged as a crucial pathway for renewable fuel production. Lignin, constituting 10–35% of woody biomass, represents a significant and largely untapped sustainable feedstock. Despite the potential of lignin, a substantial portion of this lignocellulosic residue remains unused, with approximately 60% considered waste. This study addresses the challenge of underutilized lignin by introducing an innovative approach to its hydrogenolysis. Despite their potential, existing hydrogenolysis methods face obstacles such as complexity, high cost, and the need for high temperatures or pressures. Herein we report a noncatalytic nonthermal hydrogen plasma method for lignin hydrogenolysis, conducted under ambient temperature and pressure conditions. Our method proves to be highly effective in breaking lignin bonds, achieving complete conversion, and generating valuable gaseous and bio-oil products including methane and aromatic dimers and monomers obtained from guaiacyl and syringyl units within the lignin structure. Our results showed an increase in gaseous products, especially methane, and aromatic monomer yields, as well as a reduction in total bio-oil and biochar yields and lignin functional groups by increasing reaction time, input power, and H_2 partial pressure. This research confirms the considerable promise of utilizing noncatalytic nonthermal hydrogen plasma-assisted hydrogenolysis as an effective technique for producing gaseous and liquid fuels from lignin.

1. Introduction

With the ever-increasing demand for energy and the alarming depletion of petroleum resources, there is an urgent need to shift toward sustainable energy sources [1–3]. Lignocellulosic biomass, due to its abundant presence and renewable nature, emerges as a promising solution. Composed primarily of cellulose, hemicelluloses, and lignin, lignocellulose has advantages such as local availability and carbon neutrality [4,5]. Cellulose and hemicellulose are polysaccharides that can be saccharified, fermented, or chemically processed to produce products, while lignin is collected as residual waste [6–8]. In many instances, this lignin waste or residue is typically utilized as a source of heat or power, but approximately 60 % of the lignin still goes unused and remains as waste [9]. Therefore, lignin, accounting for 10–35 % of woody biomass, holds immense potential as the only large-volume sustainable feedstock for aromatic chemicals in nature [4]. C-O and C–C bonds, such as 4-O-5, α-O-4, β-O-4, β-1, β-β, and 5–5 bonds, serve as bridges between these aromatic units. Among these bonds, the number of C-O (47–72 %) bonds exceeds that of C–C bonds (28–35 %), while their bond dissociation energies (BDEs) are lower than C–C bonds [10–12]. Due to the presence of a large number of aromatic units in the structure of lignin, the depolymerization of lignin into value-added chemicals and fuels is worth investigating. However, the complex structure of the lignin makes its valorization challenging [13–15].

Compared to other possible approaches for the depolymerization of lignin such as pyrolysis, oxidative depolymerization, enzymatic depolymerization, and acid-induced techniques [16–19], the hydrogenolysis of lignin is considered a highly promising technique for efficiently depolymerizing lignin and generating phenolic monomers with exceptional yields [20,21]. This approach employs mild reaction conditions,

* Corresponding author.
E-mail address: zmpeng@sc.edu (Z. Peng).

https://doi.org/10.1016/j.cej.2024.157776
Received 1 July 2024; Received in revised form 20 October 2024; Accepted 17 November 2024
Available online 19 November 2024

minimizing undesired condensation reactions and coke formation [22]. The catalytic hydrogenolysis of lignin has proven to be a highly effective method for obtaining aromatic chemicals with high selectivity and relatively good yield [23]. Different noble metals such as palladium (Pd) [24,25], rhodium (Rh) [26], ruthenium (Ru) [27], and platinum (Pt) [5,28] have been investigated by researchers for the hydrogenolysis of lignin. However, even though noble metal catalysts have demonstrated favorable performance in converting lignin, their high price and undesirable effects, such as excessive hydrogenation of the aromatic ring, hinder their widespread application and large-scale preparation [23,29]. On the other hand, it has been shown that cheaper catalysts such as transition metals are not as effective as noble metal catalysts in producing lignin-derived oils and monomeric phenols [30]. Lan et al. showed that during the catalytic hydrogenolysis of lignin, the deactivation of Ni/C and Ru/C catalysts can happen very fast due to the formation of carbonaceous products [31].

Researchers have extensively investigated solvent-based systems for the catalytic hydrogenolysis of lignin, focusing on aqueous solutions, alcohol solvents, and composite solvent systems [32]. Water, being cheap, non-toxic, and stable, appears as an attractive choice for this purpose [32,33]. However, it has some disadvantages including poor lignin solubility and limited hydrogen supply capacity. Consequently, most aqueous solvent systems need the addition of other additives or demand more complex catalyst designs to be effective [32]. On the other hand, alcohol solvents, such as methanol, ethanol, isopropanol, and ethylene glycol, have shown promise due to their ability to enhance the solubility of depolymerizing intermediates, reduce char formation, and provide an in-situ hydrogen source [32,34]. Yet, the effectiveness of these solvents is strongly dependent on the choice of catalyst, and the use of pure alcohol solvents as hydrogen donors can impact the cost-effectiveness of the process [32]. To address the limitations of single-solvent systems, researchers have been recently exploring composite solvent systems due to their potential to facilitate lignin hydrogenolysis and improve the selectivity of desired products. However, several crucial factors must be considered when employing these systems, including their ability to improve the catalytic activity of the reaction system, the stabilization of hydrocracking products of lignin, and the greenness and economic feasibility of these solvent systems [32]. Generally, the key drawback of using various hydrogen donor solvents in lignin hydrogenolysis is the partial integration of solvent or solvent fragments into final products. Moreover, in an industrial context, an efficient solvent-recycling strategy is crucial [35]. Therefore, some researchers have employed hydrogen gas as the hydrogen source, but this approach adds complexity and expense due to high hydrogen pressure and temperature requirements [36].

The unique chemistry and high reactivity of nonthermal plasma (non-equilibrium plasma) offer great potential to overcome kinetic and thermodynamic barriers in biomass conversions. Recently, nonthermal plasma has been explored as a promising strategy for rapid biomass conversion under mild conditions [37]. Compared to thermal plasmas, nonthermal plasma stands out due to its lower required energy to form and equipment costs [38]. There are several types of nonthermal plasmas, including Glow Discharge (GD), Microwave Discharge (MD), Corona Discharge (CD), and Dielectric Barrier Discharge (DBD). GD allows for uniform surface modifications and effective oxidation of materials. MD offers benefits due to its high energy efficiency, enabling the rapid production of materials with diverse properties. DBD has been noted for its versatility, as it can operate at both atmospheric and sub-atmospheric pressures [39]. DBDs represent a specialized configuration of electrode-based plasma reactors, primarily designed for low-temperature processing at atmospheric pressure. DBDs consist of two electrodes—one high-voltage and one grounded—separated by at least one dielectric material [40]. While DBD, GD, and MD plasmas have demonstrated higher lignin conversion rates than CD, challenges such as low energy efficiency and coke formation persist. However, DBD-based reactions offer a significant advantage over conventional methods due to their faster reaction times and the absence of high hydrogen pressures or extreme temperatures typically required for hydrogenolysis. Moreover, unlike low-pressure nonthermal plasmas, DBD reactors, operating at atmospheric pressure, further simplify the process and make continuous processing possible [38]. Compared to conventional thermal or solvent-based methods, nonthermal plasma offers several advantages, including lower operational temperatures, ambient pressure conditions, rapid processing times, and the straightforward implementation of reactions. Nonthermal plasma-assisted upcycling reactions have been shown to provide the energy needed for biomass decomposition through high-energy species like ions, electrons, and free radicals, rather than relying on thermal energy. This approach overcomes the limitations of slow heating and reaction rates [41]. Furthermore, in the case of polymer hydrogenolysis, nonthermal H_2 plasma significantly favors reaction thermodynamics, accelerating reaction kinetics and efficiently breaking down polymer bonds within minutes, much faster than conventional hydrogenolysis methods [42].

In this study, we present a novel strategy that utilizes nonthermal H_2 plasma in a DBD tubular reactor to enable the efficient hydrogenolysis of lignin under ambient temperature and pressure conditions, and investigate the effects of three main parameters including reaction time, input power, and H_2 partial pressure on the lignin conversion and yield of different products. The nonthermal H_2 plasma creates a distinct environment capable of producing highly reactive hydrogen species, mainly in the form of ions and radicals. These species play a crucial role in breaking the C-O and C–C bonds within the lignin structure (Figure S1), thereby facilitating reactions that would normally be challenging under mild reaction conditions. Unlike solvent and thermal-based methods, the non-thermal plasma method does not require high temperatures or H_2 pressure for the efficient hydrogenolysis reaction. Moreover, this method significantly reduces the probability of contamination or the addition of impurities to the final products of the reaction. Another important point regarding using non-thermal H_2 plasma for the hydrogenolysis of lignin is that it takes a dramatically shorter time to cleave bonds within the lignin structure compared to other methods, making it a fast approach for lignin hydrogenolysis. Moreover, one of the very important features of this method is the absence of catalysts, which can make this approach more cost-effective and less complicated compared to other methods which have been reported by other researchers up to this point. Finally, to the best of our knowledge, a thorough investigation of the gaseous products resulting from the hydrogenolysis of lignin has not been undertaken; therefore, the present study thoroughly investigates these gas products.

2. Experiments

2.1. Materials

Alkali lignin (Sigma-Aldrich, USA) powder was used for the nonthermal plasma-assisted hydrogenolysis reaction. Quartz wool (Thermo Fisher Scientific, UK) was used to fix the lignin pellets inside the DBD reactor. H_2 (99.999 %) and Ar (99.999 %) gases were purchased from Airgas. After the hydrogenolysis reaction, the bio-oil product was collected using acetone (≥99.5 %, Sigma-Aldrich, USA). Next, deuterated dimethylsulfoxide (DMSO-d_6) (99.9 %, Cambridge Isotope Laboratories, Inc., USA) was used as the solvent to prepare the samples for the nuclear magnetic resonance (NMR) spectroscopy, and 2,5-dihydroxybenzoic acid (Bruker, Germany) and acetonitrile (99.9 %, Sigma-Aldrich, USA) were used as the matrix and solvent, respectively, to prepare the samples for the matrix-assisted laser desorption/ionization-time of flight (MALDI-TOF) mass spectrometry. In order to analyze the biochar using the Fourier transform infrared (FTIR), it was mixed with potassium bromide (KBr) (Thermo Fisher Scientific, India).

2.2. Plasma-assisted hydrogenolysis of lignin

Plasma-assisted hydrogenolysis experiments were carried out using a quartz tube reactor (ID: 13 mm) equipped with a dielectric barrier discharge (DBD) plasma generator to assist in the hydrogenolysis of lignin through nonthermal plasma. Cold hydrogen plasma was generated in the plasma generation zone (Fig. 1) within the reactor. The volume of the plasma zone was approximately 4 cm^3. For each experiment, 900 mg lignin pellets with a size of 125–250 μm were placed inside the DBD reactor. A hydrogen flow rate of 70 ml/min, hydrogen partial pressure of 101 kPa, 70 W plasma input power, and reaction time of 30 min were the standard reaction conditions, unless stated otherwise. To investigate the effects of reaction time, input power, and H_2 partial pressure on the reaction properties, the reaction time (5, 10, 15, 20, and 30 min), input power (30, 50, and 70 W), and H_2 partial pressure (50, 70, 100 kPa) parameters were systematically varied. All reactions under different reaction conditions were repeated three times for reliability check and statistical result analysis.

The weight reduction method was primarily employed to measure the mass of the gas, bio-oil, and biochar products. For the gas product, the weight loss of the packed reactor before and after the reaction was measured. The bio-oil product was extracted from the liquid–solid mixture in the reactor using acetone as the extractant. The remaining solid residues were a mixture of biochar and quartz wool. Therefore, the weight of the biochar was determined by calculating the difference between the weight of the quartz wool and the solid residues. Likewise, the weight of the liquid product was calculated by subtracting the weight of the solvent from the total weight of the solution. In case the conversion was not 100 %, the unreacted lignin was separated from the biochar by adding DMSO to the solid residue. The unreacted lignin dissolved in the DMSO, while the biochar, being insoluble in DMSO, precipitated and was filtered for separation. Subsequently, the DMSO was evaporated to collect and weigh the unreacted lignin.

The conversion (X, %) and product distribution (Y, wt%) were calculated by the following equations:

$$X = \frac{m_L - m_{RL}}{m_L} \times 100\% \quad (1)$$

$$Y = \frac{m_{gas}/m_{bio-oil}/m_{biochar}}{m_L} \times 100\% \quad (2)$$

where m_L, m_{RL}, m_{gas}, $m_{bio\text{-}oil}$, and $m_{biochar}$, represent the mass of lignin, residual lignin, gas, bio-oil, and biochar products, respectively.

2.3. Product analysis and characterization

As shown in Fig. 1, the end of the DBD tubular reactor, wherein the lignin hydrogenolysis reaction takes place, was connected to an online Universal Gas Analyzer 300 to analyze and quantify the gas products as they are produced. The gas products were also analyzed by in-situ Fourier transform infrared (FTIR) spectroscopy with Nicolet 6700 IR spectrometer to confirm data obtained from the gas analyzer and show the evolution of different gas products during H_2 plasma-assisted hydrogenolysis of lignin.

Lignin and bio-oil products after H_2 plasma-assisted hydrogenolysis reaction were analyzed by proton nuclear magnetic resonance (^{1}H NMR) using Bruker Avance III-HD 400 MHz. For this purpose, bio-oil products were dissolved in DMSO-d_6 with a 10 mg/ml concentration. Next, bio-oil products were characterized with matrix-assisted laser desorption/ionization time-of-flight mass spectroscopy (MALDI-TOF) using a Bruker Ultraflex II MALDI-TOF/TOF instrument. Both bio-oil products and 2,5-dihydroxybenzoic acid, which was used as the matrix, were dissolved in acetonitrile with concentrations of 0.5 mg/ml and 3 mg/ml, respectively. 0.5 μl of bio-oil solution and 0.5 μl of matrix solution were dropped onto the sample plate spot and dried in air at room temperature. Positive ion MALDI-TOF MS spectra of bio-oil samples were recorded with reflectron detection mode. Accelerating voltage, laser intensity, and overall laser shots were 20 kV, 50 %, and 5000, respectively. The detection range was between 50–1600 Da.

Lignin and biochar products were characterized by ex-situ FTIR spectroscopy with Nicolet 6700 IR spectrometer in diffuse reflectance IR Fourier-transform spectroscopy (DRIFTS) mode under ambient conditions. The spectra were recorded by collecting 32 scans with a resolution of 2 cm^{-1}. No specific correction was applied. CHNS/O elemental analyzer (Perkin Elmer PE2400-Series II) and x-ray absorption spectroscopy (XAS) (Beamline 7.3.1 at the ALS) analysis were also employed to compare the structure of unreacted lignin to the biochar left at the end of the hydrogenolysis reaction.

3. Results and discussion

3.1. Effect of reaction parameters on lignin conversion and product distribution

The non-thermal plasma-assisted hydrogenolysis of lignin yielded gas, bio-oil, and biochar products. Fig. 2 illustrates the influences of reaction time, input power, and H_2 partial pressure on lignin conversion

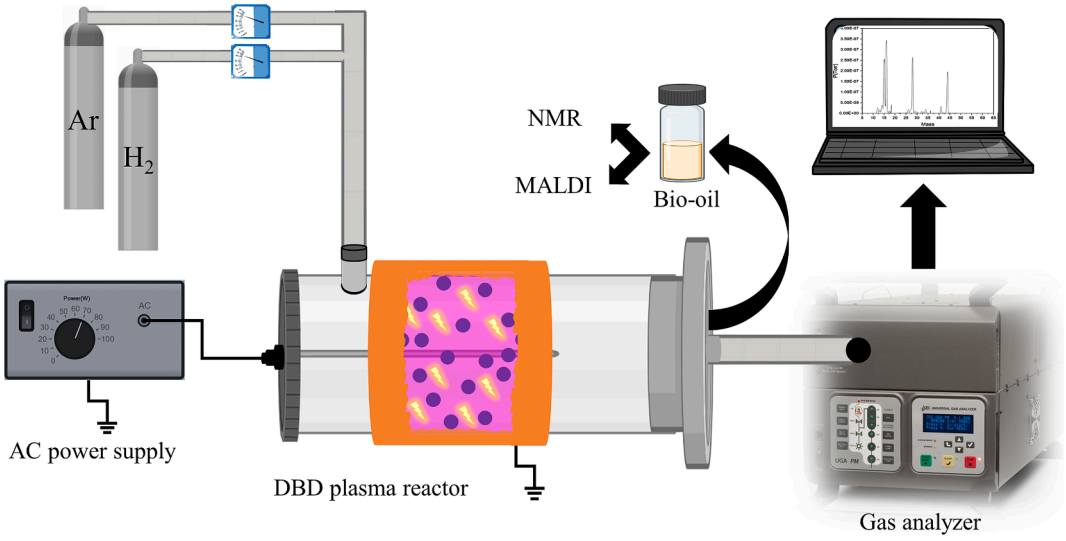

Fig. 1. Schematic of the DBD reaction system for nonthermal H_2 plasma-assisted lignin hydrogenolysis.

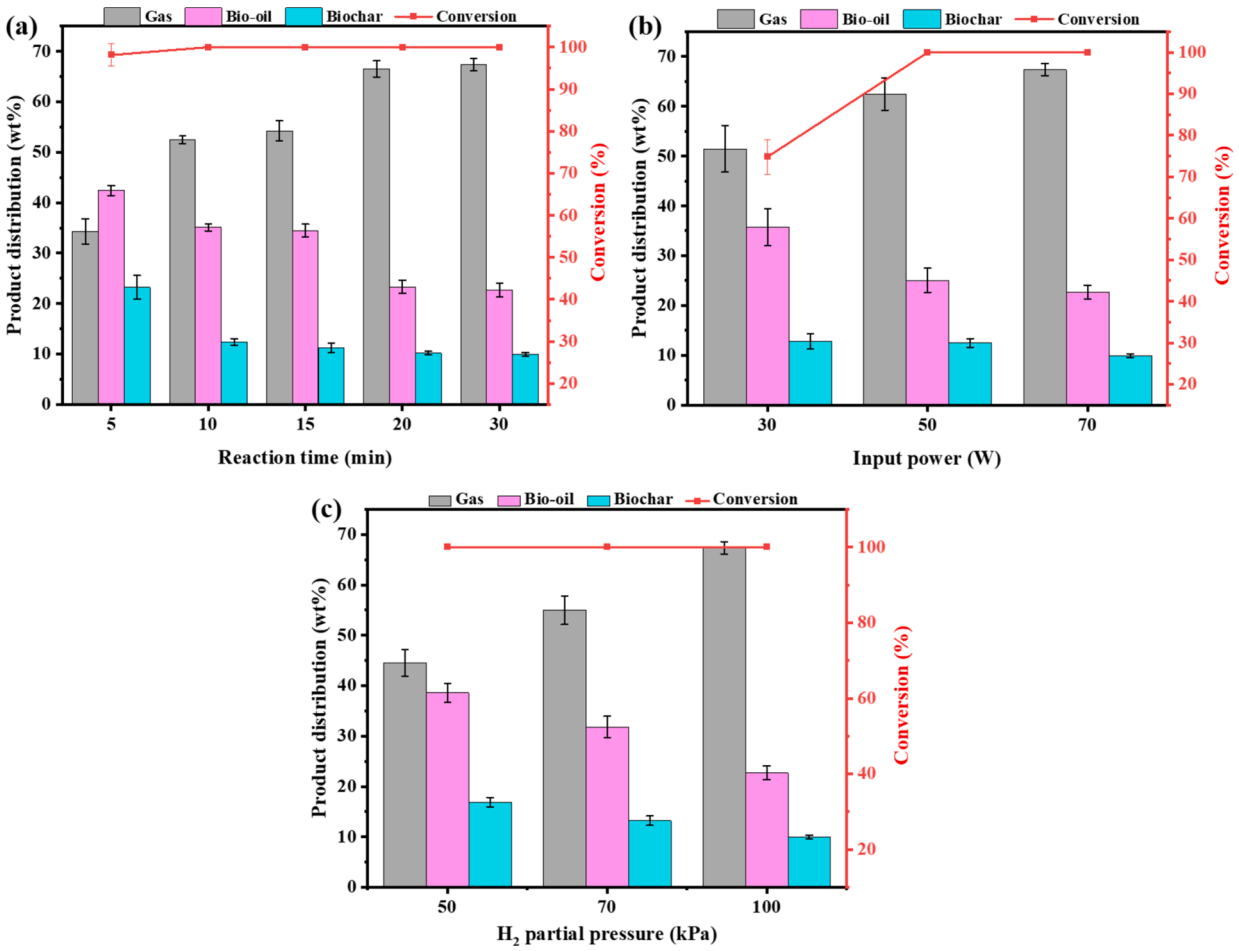

Fig. 2. The effect of (a) reaction time (input power = 70 W and H_2 partial pressure = 100 kPa), (b) input power (reaction time = 30 min and H_2 partial pressure = 100 kPa), and (c) H_2 partial pressure (reaction time = 30 min and input power = 70 W) on the conversion and yield of gaseous, bio-oil, and biochar products in nonthermal H_2 plasma-assisted lignin hydrogenolysis.

and the yield of different products. According to Fig. 2(a), it is evident that all reaction times achieved 100 % lignin conversion, except for the 5-minute reaction for which the conversion was around 98 %, indicating the rapid reaction kinetics which is significantly faster than conventional methods. An increase in the reaction time leads to a decrease in the yield of bio-oil and biochar products while simultaneously an increase in the yield of gas products. This can be inferred that an extension of the reaction time leads to the occurrence of side reactions within the initially formed bio-oil and a small portion of biochar products during hydrogenolysis and promotes their transformation into gaseous compounds by cleaving various bonds within the structures, as elaborated in the subsequent sections. As it can be seen in Fig. 2(a), after 30 min of reaction, the yield of biochar drops below 10 wt%. However, in some research investigating the catalytic hydrogenolysis of lignin the yield of biochar is significantly higher. For example, Toledano et al. studied the microwave-assisted catalytic depolymerization of lignin via mild hydrogen-free hydrogenolysis using different supported metal nanoparticles on mesoporous Al-SBA-15 including nickel (2, 5 and 10 wt%), palladium (2 wt%), platinum (2 wt%) and ruthenium (2 wt%) where the biochar yield at the end of the hydrogenolysis reaction was more than 35 % [43].

Fig. 2(b) depicts the impact of input power on lignin conversion and product yields in nonthermal plasma-assisted hydrogenolysis. With a fixed 30 min reaction time and 100 kPa H_2 partial pressure, the conversion achieved approximately 75 % at a lower input power of 30 W and reached 100 % when the power was increase to 50 W and above. This highlights the pivotal role of input power in the lignin hydrogenolysis rate and consequently the conversion. However, it should be noted that a higher input power increases electrical energy consumption that would lead to a higher operational cost. Thus, there exists a trade-off between the lignin conversion and the electrical energy consumption. However, similar studies using DBD reactors have reported significantly lower conversion rates, even at higher input powers. For instance, L. Liu et al. investigated the effect of input power in a nonthermal DBD reactor on model biomass conversion, achieving a maximum conversion of 90 % at 90 W and 300 °C. In contrast, our results demonstrate that with nonthermal plasma-assisted hydrogenolysis, it is possible to achieve 100 % conversion at lower input powers without the need for external heating [44].

In terms of product yields, the rise in input power showed a comparable effect to that of reaction time. Increasing input power resulted in a gradual increase in the gas product yield, which maximized at around 67 % at 70 W. Conversely, the bio-oil and biochar yields decreased with the input power, reaching approximately 22.7 % and 9.9 % respectively at 70 W. These results suggest a higher input power, which generates more intense hydrogen plasma, favors the conversion of the bio-oil and a small portion of biochar products into the gas molecules [45].

Fig. 2(c) examines the influence of H_2 partial pressure on lignin hydrogenolysis, with reaction time and input power fixed at 30 min and 70 W. 100 % lignin conversion was obtained with all tested H_2 partial pressures (50, 70, and 100 kPa), emphasizing the fast reaction mechanism. Meanwhile, more gas products and less bio-oil and biochar products were resulted with an increase in the H_2 partial pressure, which can be attributed to a higher concentration of hydrogen plasma that

further promotes the hydrogenolysis process.

Lissajous diagrams were utilized to demonstrate the influence of H_2 partial pressure on the formation of nonthermal plasma within the DBD reactor. As shown in Figure S2, the results clearly indicate that the addition of hydrogen leads to an increase in the area enclosed by the Lissajous diagram through increase in both plasma voltage and charge. The larger area indicates higher plasma power, which can be correlated with a higher concentration of active species in the plasma. The higher voltage range for the case of hydrogen is due to the higher breakdown voltage requirement of hydrogen molecules compared to argon. A cross comparison of the three different Lissajous diagrams shows that for the same voltage (vertical red line), the charge is much larger as hydrogen is introduced into the system (horizontal lines). Even though the ionization potential is lower for argon, atmospheric argon generally produces only Ar^+ through direct electron impact which then with heavy particle collision in atmospheric pressure forms Ar_2^+ (dimer ions). Whereas hydrogen generates H^+ and H_2^+ through electron impact, these then collide with H_2 to form H_3^+ [46–48]. Therefore, the ionization kinetics of monoatomic argon and diatomic hydrogen differ significantly, and the effect of H_2 partial pressure on the nonthermal plasma is clearly visible in the Lissajous diagrams.

Nonthermal H_2 plasma can achieve 100 % lignin conversion under most reaction conditions, whereas catalytic and thermal upcycling methods reported in the literature typically show lower conversion rates. For instance, Song et al. reported a 50 % conversion of lignin through hydrogenolysis using Ni-based catalysts and common alcohol solvents [49]. Although metallic catalysts can selectively convert lignin into specific chemicals, challenges such as the high cost of noble metals, catalyst deactivation, and limited conversion rates (typically around 50–60 %) restrict their widespread application in lignin depolymerization [50]. Hdidou et al. achieved approximately 60 % lignin conversion by depolymerizing polymer lignin models in water at 200 °C under 100 MPa with 10 % O_2 using cobalt-iron mixed oxides as catalysts [51]. Wu et al. reached a maximum lignin conversion of 87 % by pyrolyzing lignin at 600 °C for 4 h in a nitrogen atmosphere using an embedded Ni–Mo/C catalyst [52]. Therefore, compared to other methods investigated by researchers, nonthermal H_2 plasma can achieve 100 % lignin conversion at significantly lower temperatures and pressures and shorter reaction times without the need for any catalysts.

3.2. *Effect of reaction parameters on the gas products*

The gas products were analyzed in real-time during the hydrogenolysis reaction using a gas analyzer (FigureS3-S5) and were characterized using FTIR (Figure S6). Four primary products, namely CH_4, CO_2, CO, and H_2O, were identified (Fig. 3). The generation of CH_4 likely stems from the cleavage of methoxy functional group in lignin and mainly bio-oil product, formed rapidly during the hydrogenolysis reaction [53,54]. In this process, hydrogen species can target the oxygen atom within the methoxy group, thereby disrupting the methoxy bond and generating methyl intermediate that would continue to be hydrogenated to CH_4 as the final product. Nonetheless, additional contributors to CH_4 formation may be present. It has been reported that biochar, predominantly comprised of carbon, can react with hydrogen, leading to

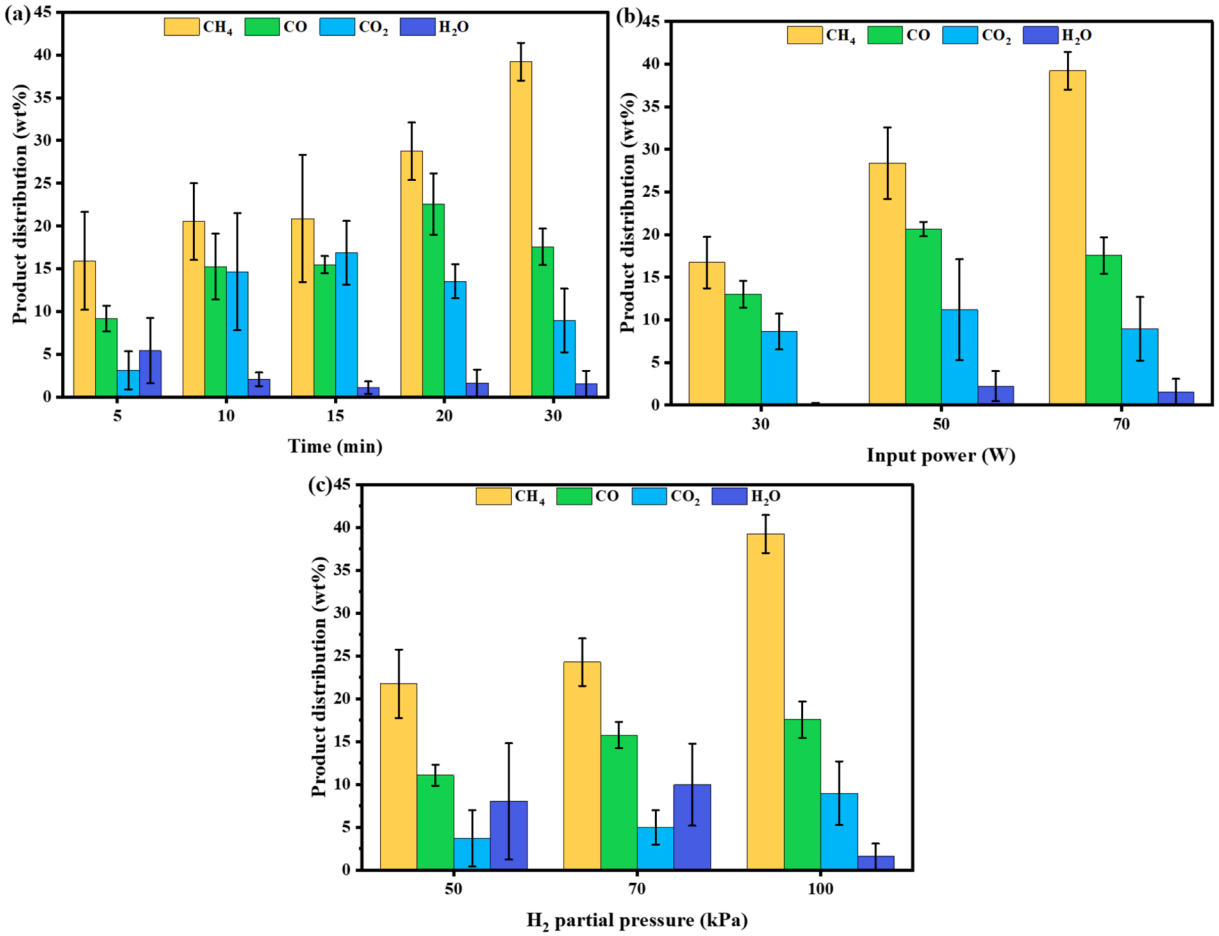

Fig. 3. The effect of (a) reaction time (input power = 70 W and hydrogen partial pressure = 100 kPa), (b) input power (reaction time = 30 min and hydrogen partial pressure = 100 kPa), and (c) H_2 partial pressure (reaction time = 30 min and input power = 70 W) on the yield of different gas products of noncatalytic nonthermal plasma-assisted hydrogenolysis of lignin.

the production of CH_4 (Eq. (3) [53].

$$C(s) + H_2(g) \rightleftharpoons CH_4(g) \quad (3)$$

CO can be produced from various distinct functional groups through several mechanistic pathways. Notably, it can be generated through the cleavage of etheric bonds, such as α-O-4 and β-O-4, characterized by weak intermolecular bonding and the decarbonylation process occurring on the C_3 side-chain [53,54]. Additionally, its formation may also stem from the cleavage of aromatic-oxygen bonds, such as methoxy and phenolic groups, and the secondary cracking of volatiles [53]. In the case of CO_2 production, the main sources are notably traced back to the presence of carboxyl (–COO^-) and ester (–CO-O-R) functional groups within the bio-oil structure produced during the lignin hydrogenolysis reaction [53,54]. However, decarboxylation reactions play the most important role in the formation of CO_2 during the hydrogenolysis of the lignin [53–55]. The primary origin of water vapor during the lignin hydrogenolysis is attributed to the intrinsic water impurity content present within the lignin powder according to the information provided by the supplier (Sigma Aldrich). The absorbed water can be gradually released as water vapor during the hydrogenolysis reaction.

As can be seen in Fig. 3, changing reaction time, input power, and H_2 partial pressure affected the product distribution. Generally, the increase in all these parameters resulted in a higher yield of CH_4. This shows a pronounced sensitivity of CH_4 production to all these reaction parameters. On the other hand, the yields of CO_2 and CO first increased by increasing the reaction time up to 15 min and 20 min, respectively, and input power up to 50 W and then decreased by further increasing these parameters. Initially, as the reaction time and input power increase, more opportunities are created for the hydrogenolysis process to occur. This could lead to enhanced cleavage of different functional groups in lignin and produced bio-oil, releasing a higher quantity of products, including CH_4, CO, and CO_2. However, as the reaction progresses and reaction pathways become saturated, the efficiency of further hydrogenolysis may decrease, contributing to a decline in the yields of CO and CO_2.

Two factors are causing the yield of CH_4 to increase constantly by increasing the reaction time and input power while causing the yields of carbon CO_2 and CO to first increase and then decrease. The first factor is the different content of various functional groups within the lignin structure. Specifically, the content of the methoxy functional group significantly surpasses the quantities of carboxyl and carbonyl functional groups (up to 10 times) [55]. Consequently, during the progression of the H_2 plasma-assisted hydrogenolysis of lignin, carboxyl and carbonyl groups are progressively converted into end products, reaching a point of complete transformation. In contrast, a residue of methoxy groups remains within the molecular structure even at higher reaction times or input powers. Consequently, in spite of the production of CO_2 and CO being constrained by the saturation of carboxyl and carbonyl groups, this residual presence of methoxy groups opens up a long-lasting pathway for methane generation. The second factor relates to the presence of biochar. As mentioned earlier, one of the pathways of the generation of CH_4 during the hydrogenolysis of the lignin process can be traced back to the interaction between solid carbon, which forms as a result of the reaction, and hydrogen. The presence of the biochar product, which is mainly composed of carbon, continues throughout the experiment, as was observed in this study. Consequently, the consistent existence of solid carbon and hydrogen results in the continuous carbon-hydrogen interaction. As a result, the ongoing production of CH_4 remains in place.

When considering the influence of H_2 partial pressure (Fig. 3c), the yield of all gas products demonstrated an increase as the H_2 partial pressure was increased from 50 kPa to 100 kPa. When the H_2 partial pressure is low, the production of hydrogen active species in the plasma region is limited. As a result, the likelihood of breaking bonds within the lignin structure, a crucial result of the hydrogenolysis process, is also limited. This is because there are fewer high-energy species available, which play a key role in initiating bond-breaking reactions.

3.3. Effect of reaction parameters on the bio-oil products

As shown in Fig. 2, bio-oil is one of the major products of nonthermal H_2 plasma-assisted hydrogenolysis of lignin. ^1H NMR and MALDI-TOF analysis were utilized to examine the bio-oil products and investigate the impacts of various parameters on them. The NMR results (Figure S9-S11) clearly demonstrate that increasing all reaction parameters resulted in a noticeable decrease in the peak intensity corresponding to the methoxy group around 3.8 ppm [56–58]. This was accompanied by a simultaneous increase in the intensities of peaks related to aliphatic (1–2 ppm) and aromatic (6.5–8 ppm) compound products [56–58]. These findings further validate the cleavage of methoxy bonds during the hydrogenolysis reaction, subsequently leading to their conversion into CH_4. Furthermore, the NMR results showed notable differences in the structure of the bio-oil as compared to lignin. The composition of the bio-oil was identified to contain a diverse range of aromatic compounds.

As a result, to gain a more detailed understanding of the bio-oil product and determine its composition, MALDI-TOF analysis was utilized. Fig. 4(and Figure S7 and S8) presents the influence of reaction time, input power, and H_2 partial pressure, respectively, on the composition of bio-oil products. According to these spectra, the important observation is that no peak was detected with an m/z value exceeding 400. Hence, it can be inferred that the process of nonthermal plasma-assisted hydrogenolysis effectively achieved the cleavage of bonds within both the lignin and the bio-oil products since the MALDI spectra of lignin usually have characteristic peaks up to $m/z = 4000$ [49,59]. Table 1 shows the general dimer structures obtained after lignin hydrogenolysis [60]. Even though the m/z values for all peaks were the same under different conditions, the increase of all three parameters increased the intensities of peaks, especially the ones attributed to monomers and products with lower m/z values ($m/z < 200$). This observation indicates that the elevation of these parameters increased the bond cleavage within the bio-oil products. Consequently, this led to the higher yield of products with smaller molecules with lower molecular weights. Utilizing the information obtained from the MALDI-TOF spectra and the specific m/z values associated with different peaks, it was possible to identify and provide a detailed analysis of the fundamental monomers and dimers that form the composition of the bio-oil (Fig. 5 and Fig. 6). The main monomeric products were guaiacol ($m/z = 124$), 4-methylguaiacol ($m/z = 138$), 4-ethylguaiacol ($m/z = 152$), Syringol $m/z = 154$), 4-propylguaiacol ($m/z = 166$), 4-methylsyringol ($m/z = 168$), 4-ethylsyringol ($m/z = 182$), and 4-propylsyringol ($m/z = 196$). Guaiacol, 4-methylguaiacol, 4-ethylguaiacol, and 4-propylguaiacol are guaiacyl (G) derivatives, and syringol, 4-methylsyringol, 4-ethylsyringol and 4-propylsyringol are syringyl (S) derivatives [43,61,62]. Fig. 4 clearly shows that the intensity of peaks related to these monomers increased by increasing the reaction time, input power, and H_2 partial pressure. Therefore, the MALDI-TOF results revealed that the main components in the bio-oil were found to be monomers and dimers which shows that the noncatalytic nonthermal H_2 plasma-assisted hydrogenolysis method was successfully capable of cleaving the bonds in lignin and bio-oil.

3.4. Effect of reaction parameters on the biochar products

FTIR was used to study the functional groups within the structures of lignin and biochar (Fig. 7, Fig. S12 and S13). The wide absorption band at 3440 cm^{-1} was linked to the stretching vibration of –OH, while the band at 2920 cm^{-1} was associated with the symmetrical vibration of C–H in the methyl group. The peak at 1703 cm^{-1} was related to the stretching vibrations of carbonyl in carboxylic acid. The vibrations of aromatic rings were indicated by peaks at 1595 and 1513 cm^{-1}. The peak at 1461 cm^{-1} was linked to the bending of methoxyl C–H and the stretching of C–C in the aromatic structure. The range between 600 and

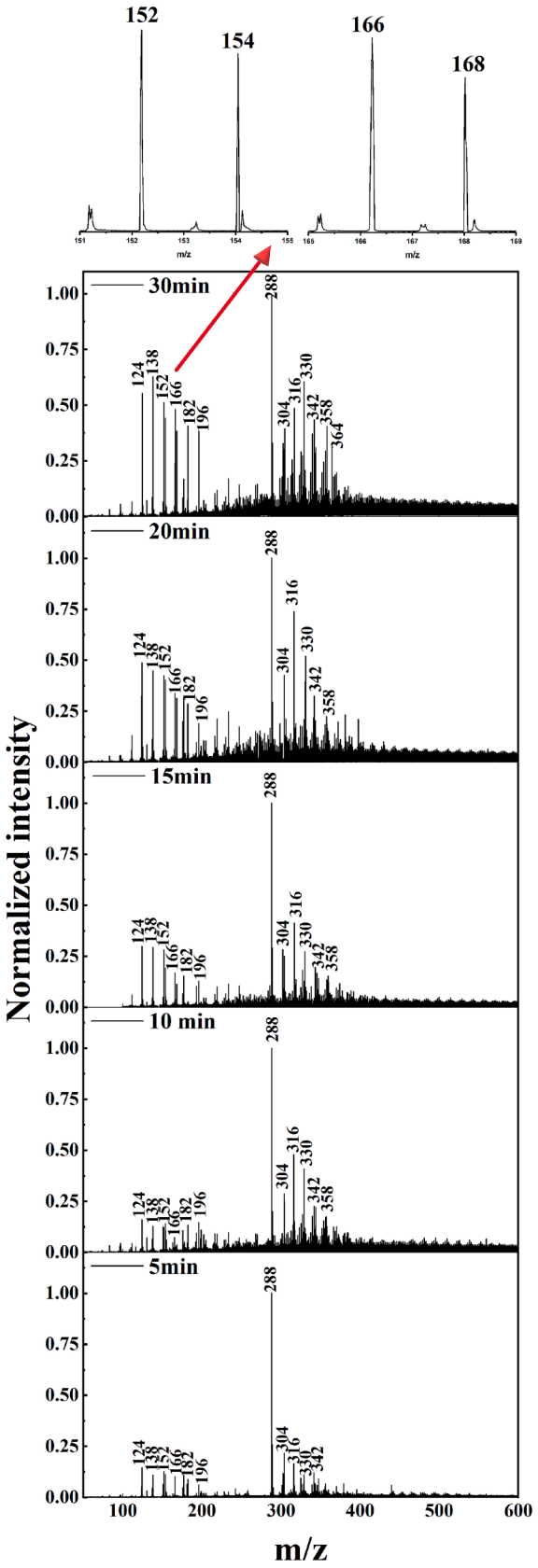

Fig. 4. MALDI spectra of bio-oil products as a function of reaction time, with input power and hydrogen partial pressure fixed at 70 W and 100 kPa.

Table 1
Structures of plausible dimeric components obtained from the lignin hydrogenolysis process.

Dimer name and bond type	Dimer general structure	Molecular weight
Diphenylethane (β-1)	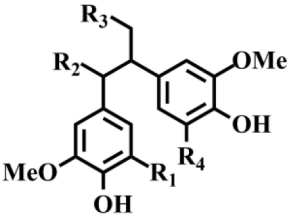	288 = [R_1 = R_2 = R_3 = R_4 = H] 318 = [R_2 = R_3 = R_4 = H, R_1 = OMe; R_1 = R_2 = R_3 = H, R_4 = OMe] 348 = [R_2 = R_3 = H, R_1 = R_4 = OMe] 304 = [R_1 = R_2 = R_4 = H, R_3 = OH] 334 = [R_1 = R_2 = H, R_3 = OH, R_4 = OMe; R_2 = R_4 = H, R_3 = OH, R_1 = OMe] 364 = [R_2 = H, R_3 = OH, R_1 = R_4 = OMe]
Phenylcoumaran (β-5)	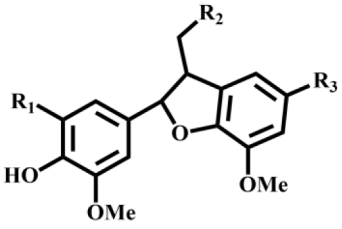	316 = [R_1 = R_3 = H, R_2 = OH] 330 = [R_1 = H, R_2 = OH, R_3 = CH_3] 344 = [R_1 = H, R_2 = OH, R_3 = CH_2CH_3] 360 = [R_1 = H, R_2 = OH, R_3 = CH_2CH_2OH] 346 = [R_1 = OMe, R_3 = H, R_2 = OH] 360 = [R_1 = OMe, R_2 = OH, R_3 = CH_3] 374 = [R_1 = OMe, R_2 = OH, R_3 = CH_2CH_3] 390 = [R_1 = OMe, R_2 = OH, R_3 = CH_2CH_2OH]
Pinoresinol (β-β)	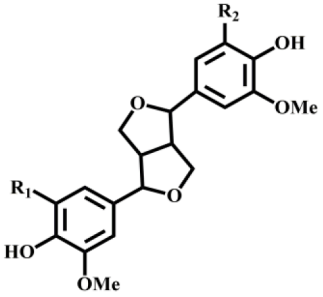	358 = [R_1 = R_2 = H] 388 = [R_1 = H, R_2 = OMe; R_2 = H, R_1 = OMe] 418 = [R_1 = R_2 = OMe]

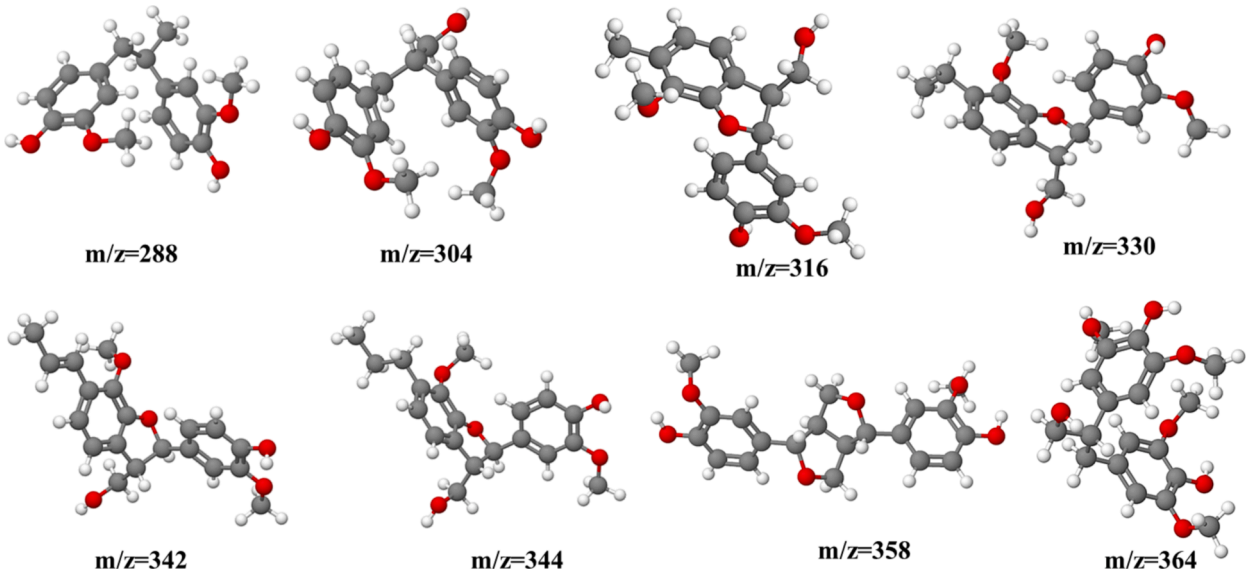

Fig. 5. Main dimers in bio-oil products (red:O, gray:C, and white:H). (For interpretation of the references to colour in this figure legend, the reader is referred to the web version of this article.)

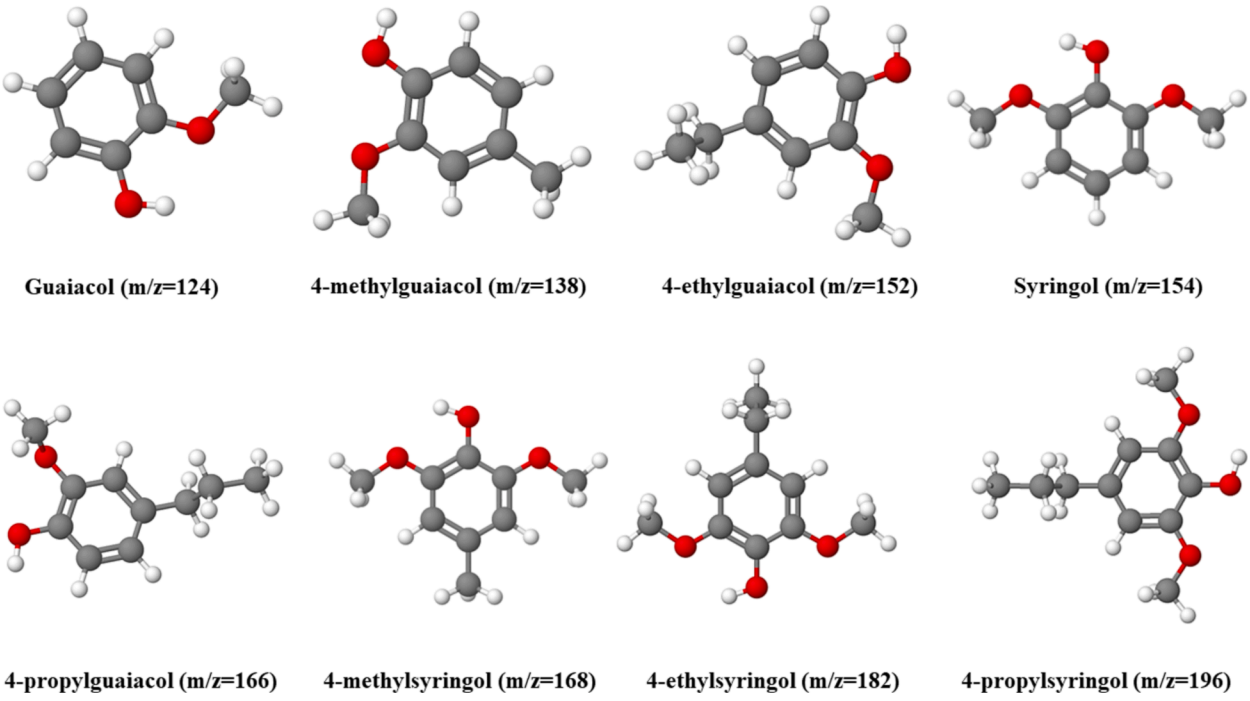

Fig. 6. Main monomers in bio-oil products (red:O, gray:C, and white:H). (For interpretation of the references to colour in this figure legend, the reader is referred to the web version of this article.)

1400 cm^{-1} was the fingerprint region [63,64]. As shown in Fig. 7a–c, all these characteristic peaks started becoming weaker by increasing the plasma-assisted hydrogenolysis reaction time, input power, and H_2 partial pressure. Therefore, the structure of biochar completely differed from lignin before the hydrogenolysis reaction, especially in the instance of biochar produced using the maximum reaction time (30 min), input power (70 W), and H_2 partial pressure (100 kPa). In this situation, all the characteristic peaks related to the lignin became notably weak, and most of them disappeared completely.

The decrease in the peak intensity related to the –OH group (3440 cm^{-1}) following hydrogenolysis indicated that the quantity of –OH groups in the biochar declined after the hydrogenolysis reaction. The peak associated with the vibration of C–H bonds in methyl groups (2920 cm^{-1}) exhibited reduced intensity in the biochar resulting from the hydrogenolysis of lignin, which shows a decrease in the presence of methyl groups, as a result of the cleavage of C3 structure and breaking of the β-O-4 bond, suggesting the generation of monophenolic compounds and the breakage of long carbon chains [65,66]. The characteristic peaks related to the vibrations of the aromatic skeletal (1595 and 1513 cm^{-1}) were detected at nearly equal intensities as those in lignin, even after a 5-minute hydrogenolysis reaction, an input power of 30 W, and an H_2 partial pressure of 50 kPa. This result showed the continued presence of aromatic rings within the biochar's structure. However, as the reaction time, input power, and H_2 partial pressure were increased, the intensity

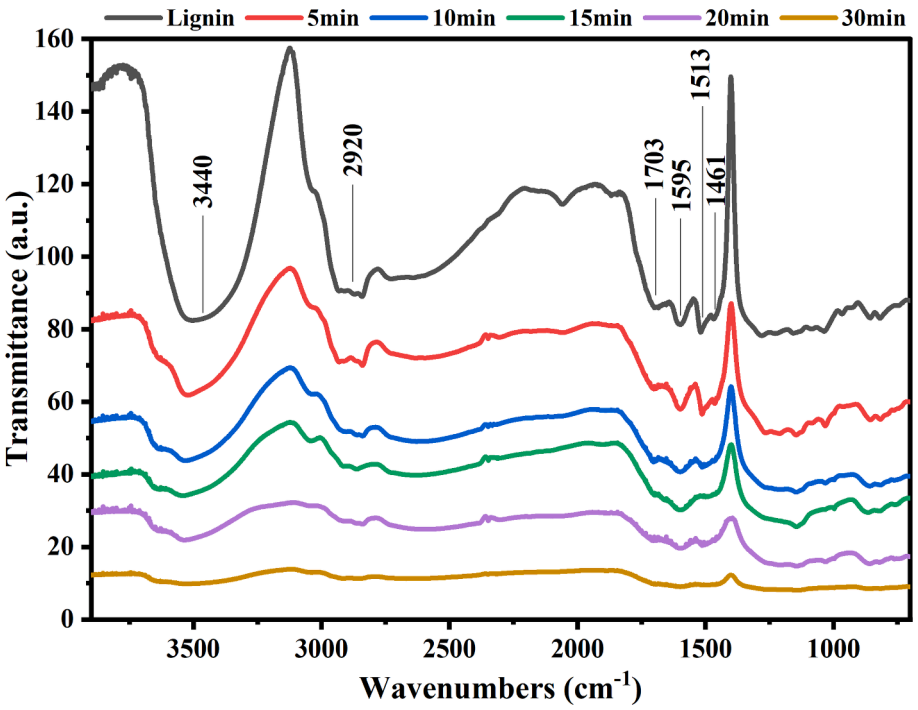

Fig. 7. FTIR spectra of biochar products as a function of reaction time, with input power and H_2 partial pressure fixed at 70 W and 100 kPa, respectively.

of these peaks gradually decreased and finally disappeared. Moreover, the intensity of the peak related to the bending of methoxyl C–H (1461 cm^{-1}) also decreased by increasing all reaction parameters and vanished at the reaction time of 10 min, the input power of 50 W, and H_2 partial pressure of 70 kPa. Finally, the peaks in the fingerprint region, which are mainly related to the guaiacol and syringol within the lignin structure, also completely disappeared which confirms the complete degradation of the lignin structure after H_2 plasma-assisted hydrogenolysis of lignin. Muvhiiwa et al. also observed that nearly all FTIR peaks corresponding to the various functional groups in wood pellets vanished following gasification and pyrolysis in a nitrogen plasma reactor [67].

XAS analysis of C K-edge (Figure S14) also clearly shows the difference between the unreacted lignin and the produced biochar during the hydrogenolysis reaction. In the lignin spectrum, three prominent 1 s → π* transition peaks are observed at 285.5 eV, 287.2 eV, and 288.8 eV, corresponding to C and H-substituted aromatic carbon, O-substituted aromatic carbon, and carboxylic groups, respectively. After 30 min of hydrogenolysis reaction, the peak related to the carboxylic group completely disappeared, and the intensity of peaks related to the C and H-substituted aromatic carbon, O-substituted aromatic carbon have significantly decreased.

The unreacted lignin and the biochar obtained after 30 min of hydrogenolysis reaction were also analyzed using a CHNS analyzer (Table. S1). Post-hydrogenolysis, the carbon content increased by approximately 20 wt%, while the hydrogen content decreased by nearly 4 wt%. Consequently, the molar ratio of carbon to hydrogen shifted from 5:6 to 3:1. Moreover, the weight percent of other elements present in the structure of lignin, mainly composed of oxygen, became almost half after the hydrogenolysis reaction. All these results clearly demonstrate the effectiveness of the non-thermal plasma-assisted hydrogenolysis method in breaking bonds within the lignin structure. Studies have shown that up to 93 % and 78 % of the biochar produced from plasma-assisted pyrolysis of woody biomass and Canna indica biomass, respectively, can consist of carbon [67,68]. However, it is important to note that the temperature used in our research is significantly lower than that employed in these studies.

3.5. Reaction pathway

Based on the analysis of hydrogenolysis products derived from lignin as presented in previous sections, a reaction pathway has been proposed to understand the mechanism behind the noncatalytic nonthermal H_2 plasma-assisted hydrogenolysis of lignin. According to Fig. 8, the cleavage of etheric bonds, including α-O-4, β-O-4, and 4-O-5 linkages, plays an important role in the generation of dimeric compounds. This phenomenon is further underscored by the fact that the rupture of C-O bonds can lead to the direct production of some monomers, such as 4-ethylguaiacol and 4-propylsyringol. Supporting this, as illustrated in Figure S1, it is evident that the bond dissociation energy (BDE) of C-O ether bonds is comparatively lower than that of C–C bonds. This difference substantiates that C-O ether bonds are preferentially susceptible to the initial impact of the nonthermal H_2 plasma-assisted hydrogenolysis reaction. The same reaction has been reported for the catalytic hydrogenolysis of lignin. Zhao et al. investigated the hydrogenolysis of lignin catalyzed by the Ni metal supported on alkaline MgO and showed that the cleavage of the ether bonds is one most important steps in converting lignin to final products during the hydrogenolysis reaction [69]. Hartwig et al. also reported that complex β-O-4 model compounds can be selectively cleaved by commercially available Pd/C catalyst through hydrogenolysis of the C–O bonds [70]. Long et al. who employed acidic ionic liquid (IL) 1-(4-sulfobutyl)-3-methyl imidazolium hydrosulfate ($[C_4H_8SO_3Hmim]HSO_4$) for liquefaction of lignin also showed that ether bonds, such as 4-O-β and 4-O-5, which connect the hydroxyphenylpropane units in lignin are first cleaved to separate the major units forming the lignin structure [71].

Notably, the ether C-O bond cleavage reactions do not culminate with the production of dimers; rather, the cleavage of C-O bonds persists as a persistent phenomenon. Importantly, it has been previously mentioned that the cleavage of C-O bonds is a main pathway for the production of methane, a primary gaseous end product. However, according to the data presented in Fig. 8, the demethylation process also has a significant role in the production of different dimers and monomers arising from the produced dimers and also converting them to lighter monomers [43]. The difference between the m/z values of monomers in MALDI spectra (Fig. 4), which are 14, clearly shows the

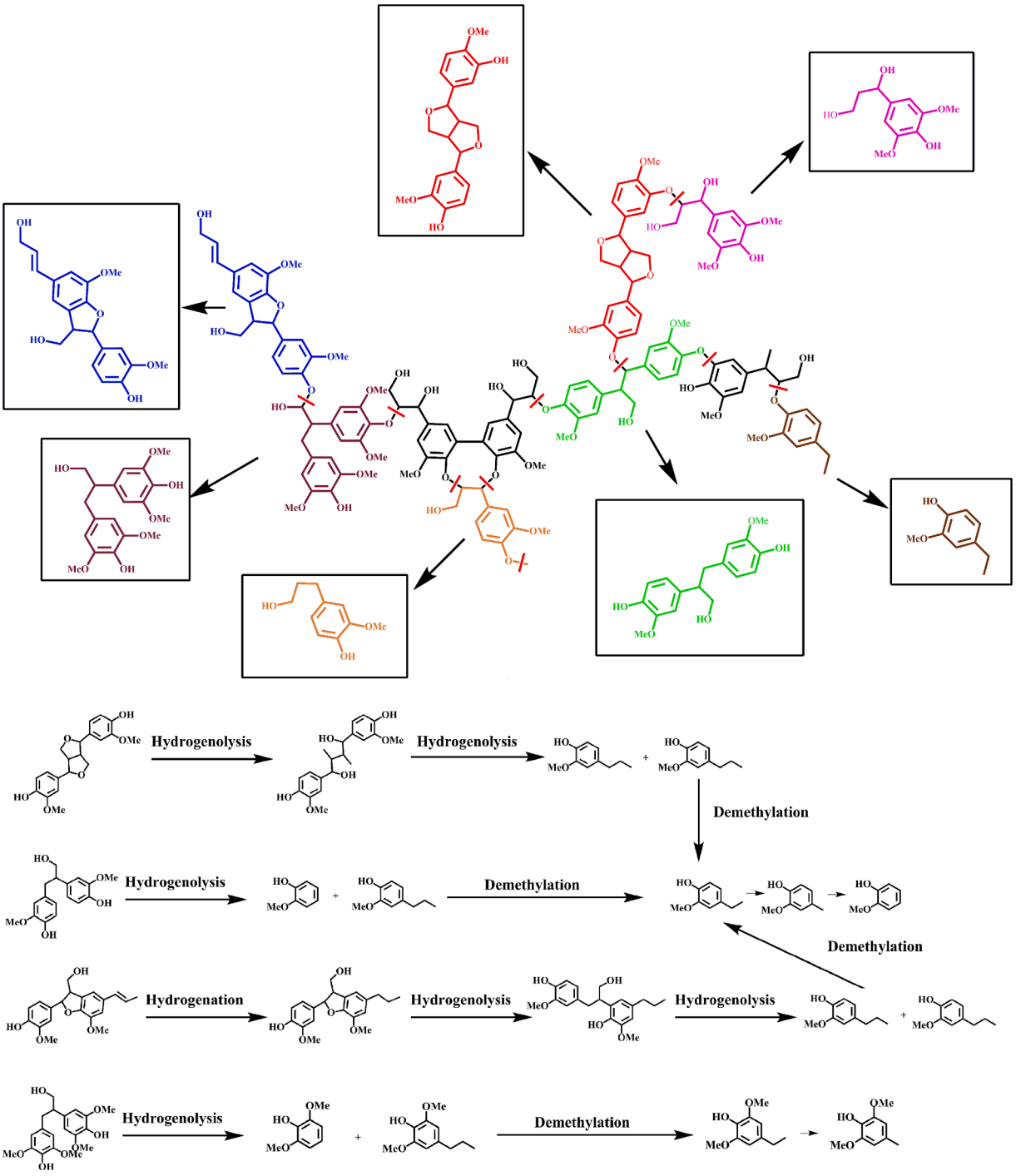

Fig. 8. Plausible reaction pathways in nonthermal H_2 plasma-assisted lignin hydrogenolysis.

demethylation process happening during the hydrogenolysis reaction. The high-energy nature of the hydrogen species generated through the employment of nonthermal H_2 plasma enables them to not only cleave O-CH_3 bonds but also disrupt CH_2-CH_3 bonds, thereby contributing to the production of CH_4 as well as lighter monomers. Pu et al. investigated lignin catalytic hydroconversion over a supported CoMoS catalyst in a semi-batch reactor and showed that hydrogen atoms can result in the demethylation reaction by removing the methyl groups [72].

According to the MALDI results (Fig. 4), it was observed that the increase in the normalized intensity of monomeric compounds outpaced the corresponding increase in the normalized intensity of dimeric species with increasing reaction time, input power, and H_2 partial pressure. This trend confirms the notion that, during the hydrogenolysis reaction, the dimers underwent a continuous transformation into lighter monomers. This trend underscores the dynamic nature of the hydrogenolysis process, where the reaction time, input power, and H_2 partial pressure can influence the reaction pathway and the extent of transformation. These observations potentially provide insight into controlling H_2 plasma-assisted hydrogenolysis process parameters to emphasize the production of desired monomeric products, which holds significance in the broader context of enhancing the efficiency and selectivity of lignin conversion.

4. Conclusion

In conclusion, the hydrogenolysis of lignin through the utilization of noncatalytic nonthermal hydrogen (H_2) plasma, conducted under ambient temperature and pressure conditions was investigated in this study, where the effects of different reaction times (5, 10, 15, 20, and 30 min), input powers (30, 50, and 70 W), and H_2 partial pressures (50, 70, and 100 kPa) on the final products were shown. The H_2 plasma-assisted hydrogenolysis exhibited remarkable efficacy in breaking lignin bonds, significantly faster than conventional methods, leading to the generation of gaseous, bio-oil, and biochar products, attaining a full conversion under all conditions except for a 5-minute reaction time (98 %) and 30 W input power (75 %). The gaseous product was composed of CH_4, CO, CO_2, and H_2O, and the bio-oil predominantly comprised aromatic monomers and dimers originating from guaiacyl and syringyl units within the lignin structure. Based on the analysis of the gaseous, bio-oil, and biochar products and the proposed reaction pathway, it appears that the breakdown of etheric bonds, including α-O-4, β-O-4, and 4-O-5 bonds, as well as lignin functional groups such as methoxy, carboxyl, carbonyl, and hydroxyl groups, significantly contributes to the formation of dimeric compounds and gaseous products. Analytical insights from the gas analyzer, NMR, and MALDI-TOF revealed a direct correlation between the increase in reaction time, input power, and H_2 partial pressure with augmented gas yields, notably CH_4, and aromatic monomers yields, alongside decreased bio-oil and biochar yields. Furthermore, FTIR spectroscopy results of biochar illustrated the progressive reduction in the intensity of characteristic peaks related to lignin functional groups with increasing reaction time, input power, and H_2 partial pressure. Ultimately, all those peaks completely disappeared, confirming the absence of lignin within the final products. Finally, it should be mentioned that even though H_2 plasma-assisted hydrogenolysis is significantly faster than conventional methods for the hydrogenolysis of lignin, the high energy consumption related to the generation of H_2 plasma may result in increased costs. Consequently, further investigations are imperative to optimize the reaction parameters and conditions, aiming to enhance energy efficiency and decrease the overall cost of this approach.

CRediT authorship contribution statement

Parsa Pishva: Writing – original draft, Validation, Investigation, Formal analysis, Data curation. **Jialu Li:** Investigation, Data curation. **Rongxuan Xie:** Investigation. **Jinyao Tang:** Investigation. **Prangan Nandy:** Investigation. **Tanvir Farouk:** Investigation. **Jinghua Guo:** Writing – review & editing. **Zhenmeng Peng:** Writing – review & editing, Supervision, Project administration, Funding acquisition, Conceptualization.

Declaration of competing interest

The authors declare that they have no known competing financial interests or personal relationships that could have appeared to influence the work reported in this paper.

Acknowledgments

We acknowledge the financial support of this work by National Science Foundation (2132178). This research used resources of the Advanced Light Source, which is a DOE Office of Science User Facility under contract no. DE-AC02-05CH11231.

Appendix A. Supplementary material

Supplementary data to this article can be found online at https://doi.org/10.1016/j.cej.2024.157776.

Data availability

Data will be made available on request.

References

[1] X. Shen, C. Zhang, B. Han, F. Wang, Catalytic self-transfer hydrogenolysis of lignin with endogenous hydrogen: road to the carbon-neutral future, Chem. Soc. Rev. 51 (2022) 1608–1628, https://doi.org/10.1039/d1cs00908g.
[2] C. Li, X. Zhao, A. Wang, G.W. Huber, T. Zhang, Catalytic transformation of lignin for the production of chemicals and fuels, Chem. Rev. 115 (2015) 11559–11624, https://doi.org/10.1021/acs.chemrev.5b00155.
[3] Y.M. Questell-Santiago, M.V. Galkin, K. Barta, J.S. Luterbacher, Stabilization strategies in biomass depolymerization using chemical functionalization, Nat. Rev. Chem. 4 (2020) 311–330, https://doi.org/10.1038/s41570-020-0187-y.
[4] X. Shen, Y. Xin, H. Liu, B. Han, Product-oriented direct cleavage of chemical linkages in lignin, ChemSusChem 13 (2020) 4367–4381, https://doi.org/10.1002/cssc.202001025.
[5] M. Cao, Y. Ma, T. Ruan, L. Li, B. Chen, X. Qiu, D. Fan, X. Ouyang, Highly efficient hydrogenolysis of lignin into monophenol over an atomically dispersed platinum catalyst, Chem. Eng. J. 485 (2024), https://doi.org/10.1016/j.cej.2024.150020.
[6] H. Kobayashi, H. Ohta, A. Fukuoka, Conversion of lignocellulose into renewable chemicals by heterogeneous catalysis, Catal. Sci. Technol. 2 (2012) 869–883, https://doi.org/10.1039/c2cy00500j.
[7] P. Mäki-Arvela, I.L. Simakova, T. Salmi, D.Y. Murzin, Production of lactic acid/lactates from biomass and their catalytic transformations to commodities, Chem. Rev. 114 (2014) 1909–1971, https://doi.org/10.1021/cr400203v.
[8] A. Yamaguchi, N. Mimura, M. Shirai, O. Sato, Bond cleavage of lignin model compounds into aromatic monomers using supported metal catalysts in supercritical water, Sci. Rep. 7 (2017), https://doi.org/10.1038/srep46172.
[9] N.L. Radhika, S. Sachdeva, M. Kumar, Lignin depolymerization and biotransformation to industrially important chemicals/biofuels, Fuel 312 (2022), https://doi.org/10.1016/j.fuel.2021.122935.
[10] Q.L. Song, Y.P. Zhao, F.P. Wu, G.S. Li, X. Fan, R.Y. Wang, J.P. Cao, X.Y. Wei, Selective hydrogenolysis of lignin-derived aryl ethers over Co/C@N catalysts, Renew Energy 148 (2020) 729–738, https://doi.org/10.1016/j.renene.2019.10.160.
[11] J. Zakzeski, P.C.A. Bruijnincx, A.L. Jongerius, B.M. Weckhuysen, The catalytic valorization of lignin for the production of renewable chemicals, Chem. Rev. 110 (2010) 3552–3599, https://doi.org/10.1021/cr900354u.
[12] S. Shao, K. Wang, J.B. Love, J. Yu, S. Du, Z. Yue, X. Fan, Water promoted photocatalytic Cβ-O bonds hydrogenolysis in lignin model compounds and lignin biomass conversion to aromatic monomers, Chem. Eng. J. 435 (2022), https://doi.org/10.1016/j.cej.2022.134980.
[13] Q. Meng, J. Yan, H. Liu, C. Chen, S. Li, X. Shen, J. Song, L. Zheng, B. Han, Self-supported hydrogenolysis of aromatic ethers to arenes, 2019. http://advances.sciencemag.org/.
[14] Q. Meng, J. Yan, R. Wu, H. Liu, Y. Sun, N.N. Wu, J. Xiang, L. Zheng, J. Zhang, B. Han, Sustainable production of benzene from lignin, Nat. Commun. 12 (2021), https://doi.org/10.1038/s41467-021-24780-8.
[15] A. Catalysis, T. Hou, N. Luo, H. Li, M. Heggen, J. Lu, Y. Wang, F. Wang, Subscriber access provided by HACETTEPE UNIVERSITESI KUTUPHANESI Yin and Yang Dual Characters of CuOx Clusters for C-C Bond Oxidation Driven by Visible Light, 2017. http://pubs.acs.org.
[16] D. Ferdous, A.K. Dalai, S.K. Bej, R.W. Thring, Pyrolysis of lignins: Experimental and kinetics studies, Energy Fuel 16 (2002) 1405–1412, https://doi.org/10.1021/ef0200323.
[17] A. Rahimi, A. Ulbrich, J.J. Coon, S.S. Stahl, Formic-acid-induced depolymerization of oxidized lignin to aromatics, Nature 515 (2014) 249–252, https://doi.org/10.1038/nature13867.
[18] J.C. Chan, M. Paice, X. Zhang, Enzymatic oxidation of lignin: challenges and barriers toward practical applications, ChemCatChem 12 (2020) 401–425, https://doi.org/10.1002/cctc.201901480.
[19] C.S. Lancefield, O.S. Ojo, F. Tran, N.J. Westwood, Isolation of functionalized phenolic monomers through selective oxidation and CO bond cleavage of the β-O-4 linkages in Lignin, Angew. Chemie – Int. Ed. 54 (2015) 258–262, https://doi.org/10.1002/anie.201409408.
[20] S. Wang, K. Zhang, H. Li, L.P. Xiao, G. Song, Selective hydrogenolysis of catechyl lignin into propenylcatechol over an atomically dispersed ruthenium catalyst, Nat. Commun. 12 (2021), https://doi.org/10.1038/s41467-020-20684-1.
[21] C. Feng, L. Xuebin, C. Wei, W. Na, J. Yanqiao, Double core–shell hollow nanocage $CuO@Co_3O_4$ for the selective hydrogenolysis of C–O bonds of lignin without external hydrogen, Chem. Eng. J. 491 (2024), https://doi.org/10.1016/j.cej.2024.152002.
[22] M. Kleinert, T. Barth, Phenols from lignin, Chem. Eng. Technol. 31 (2008) 736–745, https://doi.org/10.1002/ceat.200800073.
[23] C. Cheng, P. Li, W. Yu, D. Shen, X. Jiang, S. Gu, Nonprecious metal/bimetallic catalytic hydrogenolysis of lignin in a mixed-solvent system, ACS Sustain. Chem. Eng. 8 (2020) 16217–16228, https://doi.org/10.1021/acssuschemeng.0c05362.
[24] C. Peng, Q. Chen, H. Guo, G. Hu, C. Li, J. Wen, H. Wang, T. Zhang, Z.K. Zhao, R. Sun, H. Xie, Effects of extraction methods on structure and valorization of corn stover lignin by a Pd/C catalyst, ChemCatChem 9 (2017) 1135–1143, https://doi.org/10.1002/cctc.201601501.

[25] S. Van Den Bosch, W. Schutyser, S.F. Koelewijn, T. Renders, C.M. Courtin, B.F. Sels, Tuning the lignin oil OH-content with Ru and Pd catalysts during lignin hydrogenolysis on birch wood, Chem. Commun. 51 (2015) 13158–13161, https://doi.org/10.1039/c5cc04025f.

[26] J. Yang, L. Zhao, S. Liu, Y. Wang, L. Dai, High-quality bio-oil from one-pot catalytic hydrocracking of kraft lignin over supported noble metal catalysts in isopropanol system, Bioresour. Technol. 212 (2016) 302–310, https://doi.org/10.1016/j.biortech.2016.04.029.

[27] D. Ma, S. Lu, X. Liu, Y. Guo, Y. Wang, Depolymerization and hydrodeoxygenation of lignin to aromatic hydrocarbons with a Ru catalyst on a variety of Nb-based supports, 2019. http://www.sciencedirect.com/science/journal/18722067.

[28] D. Panke, G. Bechthold, T.E. Müller, Solvent effect in catalytic lignin hydrogenolysis, Catalysts 12 (2022), https://doi.org/10.3390/catal12060664.

[29] Z. Wang, X. Chen, Y. Sun, D. Hua, S. Yang, L. Sun, T. Li, L. Chen, Co-pyrolysis induced strong metal-support interaction in N-doped carbon supported Ni catalyst for the hydrogenolysis of lignin, Chem. Eng. J. 473 (2023), https://doi.org/10.1016/j.cej.2023.145182.

[30] J.Y. Kim, J. Park, U.J. Kim, J.W. Choi, Conversion of lignin to phenol-rich oil fraction under supercritical alcohols in the presence of metal catalysts, Energy Fuel 29 (2015) 5154–5163, https://doi.org/10.1021/acs.energyfuels.5b01055.

[31] W. Lan, Y.P. Du, S. Sun, J. Behaghel De Bueren, F. Héroguel, J.S. Luterbacher, Continuous hydrogenolysis of acetal-stabilized lignin in flow, Green Chem. 23 (2021) 320–327, https://doi.org/10.1039/d0gc02928a.

[32] K. Ye, Y. Liu, S. Wu, J. Zhuang, A review for lignin valorization: Challenges and perspectives in catalytic hydrogenolysis, Ind. Crop. Prod. 172 (2021), https://doi.org/10.1016/j.indcrop.2021.114008.

[33] D. Wang, X. Li, Y. Wang, X. Li, L. Chen, G. Li, Lignin valorization: a novel in situ catalytic hydrogenolysis method in alkaline aqueous solution, Energy Fuel 32 (2018) 7643–7651, https://doi.org/10.1021/acs.energyfuels.8b01032.

[34] R. Shu, Q. Zhang, L. Ma, Y. Xu, P. Chen, C. Wang, T. Wang, Insight into the solvent, temperature and time effects on the hydrogenolysis of hydrolyzed lignin, Bioresour. Technol. 221 (2016) 568–575, https://doi.org/10.1016/j.biortech.2016.09.043.

[35] I. Hita, P.J. Deuss, G. Bonura, F. Frusteri, H.J. Heeres, Biobased chemicals from the catalytic depolymerization of Kraft lignin using supported noble metal-based catalysts, Fuel Process. Technol. 179 (2018) 143–153, https://doi.org/10.1016/j.fuproc.2018.06.018.

[36] D. Tang, X. Huang, W. Tang, Y. Jin, Lignin-to-chemicals: Application of catalytic hydrogenolysis of lignin to produce phenols and terephthalic acid via metal-based catalysts, Int. J. Biol. Macromol. 190 (2021) 72–85, https://doi.org/10.1016/j.ijbiomac.2021.08.188.

[37] R. Zhou, R. Zhou, S. Wang, U.G. Mihiri Ekanayake, Z. Fang, P.J. Cullen, K. Bazaka, K. (Ken) Ostrikov, Power-to-chemicals: Low-temperature plasma for lignin depolymerisation in ethanol, Bioresour. Technol. 318 (2020), https://doi.org/10.1016/j.biortech.2020.123917.

[38] S. Shao, Z. Ye, J. Sun, C. Liu, J. Yan, T. Liu, X. Li, H. Zhang, R. Xiao, A review on the application of non-thermal plasma (NTP) in the conversion of biomass: catalyst preparation, thermal utilization and catalyst regeneration, Fuel 330 (2022), https://doi.org/10.1016/j.fuel.2022.125420.

[39] L. Qin, O.L. Li, Recent progress of low-temperature plasma technology in biorefining process, Nano Converg. 10 (2023), https://doi.org/10.1186/s40580-023-00386-2.

[40] P. Dimitrakellis, E. Delikonstantis, G.D. Stefanidis, D.G. Vlachos, Plasma technology for lignocellulosic biomass conversion toward an electrified biorefinery, Green Chem. 24 (2022) 2680–2721, https://doi.org/10.1039/d1gc03436g.

[41] F. Li, G. Li, B.G. Lougou, Q. Zhou, B. Jiang, Y. Shuai, Upcycling biowaste into advanced carbon materials via low-temperature plasma hybrid system: applications, mechanisms, strategies and future prospects, Waste Manag. 189 (2024) 364–388, https://doi.org/10.1016/j.wasman.2024.08.036.

[42] X. Chen, Y. Wang, L. Zhang, Recent progress in the chemical upcycling of plastic wastes, ChemSusChem 14 (2021) 4137–4151, https://doi.org/10.1002/cssc.202100868.

[43] A. Toledano, L. Serrano, A. Pineda, A.A. Romero, R. Luque, J. Labidi, Microwave-assisted depolymerisation of organosolv lignin via mild hydrogen-free hydrogenolysis: Catalyst screening, Appl. Catal. B 145 (2014) 43–55, https://doi.org/10.1016/j.apcatb.2012.10.015.

[44] L. Liu, Q. Wang, J. Song, X. Yang, Y. Sun, Dry reforming of model biomass pyrolysis products to syngas by dielectric barrier discharge plasma, Int. J. Hydrogen Energy 43 (2018) 10281–10293, https://doi.org/10.1016/j.ijhydene.2018.04.112.

[45] L. Yao, J. King, D. Wu, S.S.C. Chuang, Z. Peng, Non-thermal plasma-assisted hydrogenolysis of polyethylene to light hydrocarbons, Catal. Commun. 150 (2021), https://doi.org/10.1016/j.catcom.2020.106274.

[46] T. Farouk, B. Farouk, D. Staack, A. Gutsol, A. Fridman, Modeling of direct current micro-plasma discharges in atmospheric pressure hydrogen, Plasma Sources Sci. Technol. 16 (2007) 619–634, https://doi.org/10.1088/0963-0252/16/3/023.

[47] T. Farouk, B. Farouk, D. Staack, A. Gutsol, A. Fridman, Simulation of dc atmospheric pressure argon micro glow-discharge, Plasma Sources Sci. Technol. 15 (2006) 676–688, https://doi.org/10.1088/0963-0252/15/4/012.

[48] D. Staack, B. Farouk, A. Gutsol, A. Fridman, DC normal glow discharges in atmospheric pressure atomic and molecular gases, Plasma Sources Sci. Technol. 17 (2008), https://doi.org/10.1088/0963-0252/17/2/025013.

[49] Q. Song, F. Wang, J. Cai, Y. Wang, J. Zhang, W. Yu, J. Xu, Lignin depolymerization (LDP) in alcohol over nickel-based catalysts via a fragmentation-hydrogenolysis process, Energy Environ. Sci. 6 (2013) 994–1007, https://doi.org/10.1039/c2ee23741e.

[50] C. Chio, M. Sain, W. Qin, Lignin utilization: a review of lignin depolymerization from various aspects, Renew. Sustain. Energy Rev. 107 (2019) 232–249, https://doi.org/10.1016/j.rser.2019.03.008.

[51] L. Hdidou, L. Kouisni, B. Manoun, H. Hannache, A. Solhy, A. Barakat, Oxidative conversion of lignin over cobalt-iron mixed oxides prepared via the alginate gelation, Catal. Commun. 117 (2018) 99–104, https://doi.org/10.1016/j.catcom.2018.08.027.

[52] Y. Wu, Q. Dang, T. Wu, T. Lei, K. Wang, Z. Luo, Efficient lignin depolymerization process for phenolic products with lignin-based catalysts and mixed solvents, Energy Fuel 37 (2023) 5206–5219, https://doi.org/10.1021/acs.energyfuels.3c00063.

[53] Q. Yan, J. Li, J. Zhang, Z. Cai, Thermal decomposition of Kraft Lignin under Gas atmospheres of argon, hydrogen, and carbon dioxide, Polymers (Basel) 10 (2018), https://doi.org/10.3390/polym10070729.

[54] D. Chen, K. Cen, X. Zhuang, Z. Gan, J. Zhou, Y. Zhang, H. Zhang, Insight into biomass pyrolysis mechanism based on cellulose, hemicellulose, and lignin: Evolution of volatiles and kinetics, elucidation of reaction pathways, and characterization of gas, biochar and bio-oil, Combust. Flame 242 (2022), https://doi.org/10.1016/j.combustflame.2022.112142.

[55] Structure and Characteristics of Lignin, in: Lignin Chemistry and Applications, Elsevier, 2019: pp. 25–50. https://doi.org/10.1016/b978-0-12-813941-7.00002-3.

[56] Y. Qian, Q. Zhang, X. Qiu, S. Zhu, CO_2-responsive diethylaminoethyl-modified lignin nanoparticles and their application as surfactants for CO_2/N_2-switchable Pickering emulsions, Green Chem. 16 (2014) 4963–4968, https://doi.org/10.1039/c4gc01242a.

[57] J.S. Mun, J.A. Pe, S.P. Mun, Chemical characterization of kraft lignin prepared from mixed hardwoods, Molecules 26 (2021), https://doi.org/10.3390/molecules26164861.

[58] C. Fernández-Costas, S. Gouveia, M.A. Sanromán, D. Moldes, Structural characterization of Kraft lignins from different spent cooking liquors by 1D and 2D nuclear magnetic resonance spectroscopy, Biomass Bioenergy 63 (2014) 156–166, https://doi.org/10.1016/j.biombioe.2014.02.020.

[59] I. Dababi, O. Gimello, E. Elaloui, F. Quignard, N. Brosse, Organosolv lignin-based wood adhesive. Influence of the lignin extraction conditions on the adhesive performance, Polymers (Basel) 8 (2016), https://doi.org/10.3390/polym8090340.

[60] C. Cheng, P. Li, W. Yu, D. Shen, S. Gu, Catalytic hydrogenolysis of lignin in ethanol/isopropanol over an activated carbon supported nickel-copper catalyst, Bioresour. Technol. 319 (2021), https://doi.org/10.1016/j.biortech.2020.124238.

[61] C. Chen, P. Liu, B.K. Sharma, H. Xia, M. Zhou, J. Jiang, Insights into catalytic valorization of different lignin feedstocks into liquid fuels with microwave heating in hydrogen-donor solvents, Biomass Convers. Biorefin. 12 (2022) 3817–3826, https://doi.org/10.1007/s13399-020-00849-0.

[62] L. Dong, Y. Xin, X. Liu, Y. Guo, C.W. Pao, J.L. Chen, Y. Wang, Selective hydrodeoxygenation of lignin oil to valuable phenolics over Au/Nb2O5 in water, Green Chem. 21 (2019) 3081–3090, https://doi.org/10.1039/c9gc00327d.

[63] Z. Shi, G. Xu, J. Deng, M. Dong, V. Murugadoss, C. Liu, Q. Shao, S. Wu, Z. Guo, Structural characterization of lignin from D. sinicus by FTIR and NMR techniques, Green Chem. Lett. Rev. 12 (2019) 235–243, https://doi.org/10.1080/17518253.2019.1627428.

[64] R. Md Salim, J. Asik, M.S. Sarjadi, Chemical functional groups of extractives, cellulose and lignin extracted from native Leucaena leucocephala bark, Wood Sci. Technol. 55 (2021) 295–313, https://doi.org/10.1007/s00226-020-01258-2.

[65] D. Duan, Y. Zhao, L. Fan, L. Dai, J. Lv, R. Ruan, Y. Wang, Y. Liu, Low-Power Microwave Radiation-assisted Depolymerization of Ethanol Organosolv Lignin in Ethanol/Formic Acid Mixtures, n.d.

[66] X.-P. Ouyang, Y.-D. Tan, Q. Xue-Qing, Oxidative degradation of lignin for producing monophenolic compounds, 2014.

[67] R. Muvhiiwa, A. Kuvarega, E.M. Llana, A. Muleja, Study of biochar from pyrolysis and gasification of wood pellets in a nitrogen plasma reactor for design of biomass processes, J. Environ. Chem. Eng. 7 (2019), https://doi.org/10.1016/j.jece.2019.103391.

[68] Y. Mittal, P. Srivastava, N. Kumar, M. Kumar, S.K. Singh, F. Martinez, A.K. Yadav, Ultra-fast and low-cost electroactive biochar production for electroactive-constructed wetland applications: A circular concept for plant biomass utilization, Chem. Eng. J. 452 (2023), https://doi.org/10.1016/j.cej.2022.138587.

[69] W. Zhao, X. Li, H. Li, X. Zheng, H. Ma, J. Long, X. Li, Selective hydrogenolysis of lignin catalyzed by the cost-effective Ni Metal supported on alkaline MgO, ACS Sustain. Chem. Eng. 7 (2019) 19750–19760, https://doi.org/10.1021/acssuschemeng.9b05041.

[70] F. Gao, J.D. Webb, H. Sorek, D.E. Wemmer, J.F. Hartwig, Fragmentation of lignin samples with commercial Pd/C under ambient pressure of hydrogen, ACS Catal. 6 (2016) 7385–7392, https://doi.org/10.1021/acscatal.6b02028.

[71] J. Long, W. Lou, L. Wang, B. Yin, X. Li, $[C_4H_8SO_3Hmim]HSO_4$ as an efficient catalyst for direct liquefaction of bagasse lignin: decomposition properties of the inner structural units, Chem. Eng. Sci. 122 (2015) 24–33, https://doi.org/10.1016/j.ces.2014.09.026.

[72] J. Pu, D. Laurenti, C. Geantet, M. Tayakout-Fayolle, I. Pitault, Kinetic modeling of lignin catalytic hydroconversion in a semi-batch reactor, Chem. Eng. J. 386 (2020), https://doi.org/10.1016/j.cej.2019.122067.